Electronic Supplementary Material (ESI) for Journal of Materials Chemistry C.

Supporting information

Zipper-like molecular packing of donor-acceptor conjugated co-oligomers based on perylenediimide

Laure Biniek,[1] Pierre-Olivier Schwartz,[2] Elena Zaborova,[3] Benoit Heinrich,[2] Nicolas Leclerc,[3] Stéphane Méry,[2] Martin Brinkmann[1*]

[1] Institut Charles Sadron, CNRS, Université de Strasbourg, 23 rue du Loess, BP 84047, 67034 Strasbourg Cedex2, France.

[2] Institut de Physique et de Chimie des Matériaux de Strasbourg, 23 rue du Loess, BP 84047, 67034 Strasbourg, Cedex2, France.

[3] ICPEES, UMR 7515, ECPM, 25 rue Becquerel, 67087 Strasbourg Cedex2, France.

*** Corresponding author:** martin.brinkmann@ics-cnrs.unistra.fr

I. Experimental section.

a) Thin film orientation.

All dyads and triads used in this study were synthesized following the procedures described in reference 1.

The films of AD_0, AD_1 and ADA were prepared by doctor blading on clean glass substrates, a 4 wt% solution in chloroform at 45°C for the dyads and a 4 wt% solution in *ortho*-dichlorobenzene (*o*-DCB) at 175°C for ADA triad. Cleaning of the glass substrates was obtained by i) sonication in acetone (15 min), ii) sonication in ethanol (15 min), iii) mechanical scrubbing with a soft tooth brush using a distilled hellmanex (Hellma Gmbh) solution in deionized water and iv) sonication in deionized water (3×). The slides were subsequently dried in a flow of nitrogen.

For the alignment of the films by high-temperature rubbing, a home-made machine was used (2). It is composed of a rotating cylinder (4 cm diameter) covered by a microfiber cloth. The rubbing is performed by applying the rotating cylinder with a 2 bar pressure on the translating sample holder (1 cm/s). The sample holder can be heated to the desired temperature (100°C) during the rubbing process. The sample temperature is allowed to equilibrate for 1-2 min before rubbing. A rubbing cycle is characterized by the so-called rubbing length i.e. the length of the rubbing tissue applied on a given point of the sample. In the present case, it is 50 cm. Post-alignment thermal annealing was done in a Linkam hot stage under inert atmosphere at the 210°C, 195°C and 240°C respectively for AD_0, AD_1 and ADA for 1 min. Heating and cooling rates were 20 °C/min and 0.5 °C/min, respectively.

Oriented PTFE substrates were prepared according to the method described elsewhere (3) by sliding a PTFE rod at a constant pressure (5 bar) against a clean glass slide held at 250-300°C. The dyads films were prepared by drop casting from a solution in 4 wt% chloroform

on the PTFE substrates. The oriented films were then annealed at 235°C and 215°C (for 1 min), respectively for AD_0 and AD_1. Due to the strong dewetting of the ADA upon casting on PTFE, the ADA films were first prepared by casting onto water and subsequently transferred to the PTFE substrates prior to thermal annealing at 270°C (for 1 min).

b) Strucural analysis.

Highly oriented areas of the films were selected by optical microscopy (Leica DMR-X microscope). The films were coated with a thin amorphous carbon film and removed from the glass substrate by using either a diluted aqueous HF solution (10 wt %) or polyacrylic acid and subsequently recovered onto TEM copper grids.

TEM was performed in both bright field and diffraction modes using a Philips CM12 microscope equipped with a MVIII CCD camera (Soft Imaging System). The acquisition conditions for the Electron Diffraction (ED) patterns are similar to those reported earlier for P3HT (4). For HR-TEM imaging, a modified low dose operating mode was used as described in details elsewhere (5). The image filtering and fast-Fourier transform (FFT) analyses were performed using the AnalySiS software. Fast Fourier filtering conditions were chosen such as to minimize ghost lattice generation as explained in reference 6.

In situ annealing TEM measurements were performed by using a PW6592 sample holder and a PW6363 heating temperature controller (Phillips). To estimate beam damage of the dyad sample during the *in situ* TEM measurement, a spot size of 11 was selected. The temperature was increased by steps of 12-13°C and allowed to stabilize for 1 min at each step. In those periods, the electron beam was blanked by a shutter. After temperature stabilization, the beam shutter was opened for 2 s to acquire the ED pattern. Calibration of the reticular distances in the ED patterns was made with an oriented PTFE film.

Molecular modeling was performed on a Silicon Graphic station using the Cerius2 program. A trial-and-error procedure was used to refine the structure of AD_0, following the same methodology as used previously for poly(9,9-di-*n*-octyl-fluorene) and poly(3-hexylthiophene)) (4, 6). For each step of the trial-and-error method, the molecular geometry was optimized using the "clean" procedure of the Cerius2 3.0 Program (additional informations on this procedure are available in the User's guide on Modeling Environment).

GIXD measurements were performed at PLS-II 9A U-SAXS beamline of Pohang Accelerator Laboratory (PAL) in Korea, in the frame of the proposal number "2013-2nd-9A- 008" (SOPOELEC). Si(1 0 0) wafers (Silchem mbH, Germany) with a native oxide were used as substrate. The X-ray beam coming from the vacuum undulator (IVU) was monochromated using Si(111) double crystals and focused on the detector using K-B type mirrors. Patterns were recorded with a 2D CCD detector (Rayonix SX165). The sample-to-detector distance was about 225 mm for an energy of 11.08 keV (1.119 Å)

II. Supplementary informations.

a) High-temperature rubbing of co-oligomer films.

Alignment of mesophases can be obtained on orienting substrates such as rubbed poly(imide)s or friction-transferred poly(tetrafluoroethylene) substrates (PTFE).[7] Herein, high temperature rubbing was first chosen to align the lamellar mesophases of AD and ADA co-oligomers. Orientation is enforced via the shear forces exerted at the interface between the

film and the surface of a rubbing tissue on a rotating cylinder. The control of the film temperature during mechanical rubbing makes it possible to obtain very high alignments without resorting to an alignment substrate as illustrated for numerous conjugated polymers including poly(3-alkylthiophene)s and poly(thienothiophene)s.[8]

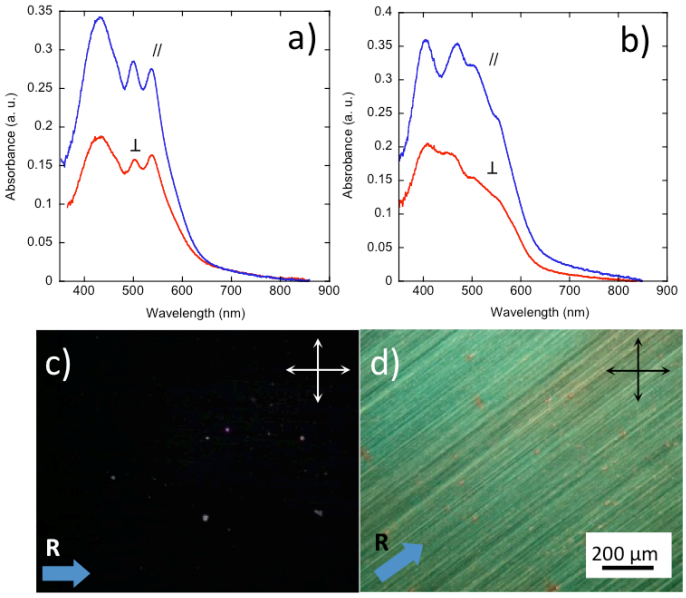

***Figure ESI 1**: UV-Vis polarized optical absorption of an AD_1 film oriented by rubbing (a) and subsequently annealed at 190°C (1 min) (b) for the incident light polarization parallel (blue curves) and perpendicular (red curves) to the rubbing direction. c) and d) POM images under crossed polarizer showing the highly oriented film of AD_1 obtained after rubbing and subsequent annealing at 190°C. The rubbing direction R is indicated by a blue arrow.*

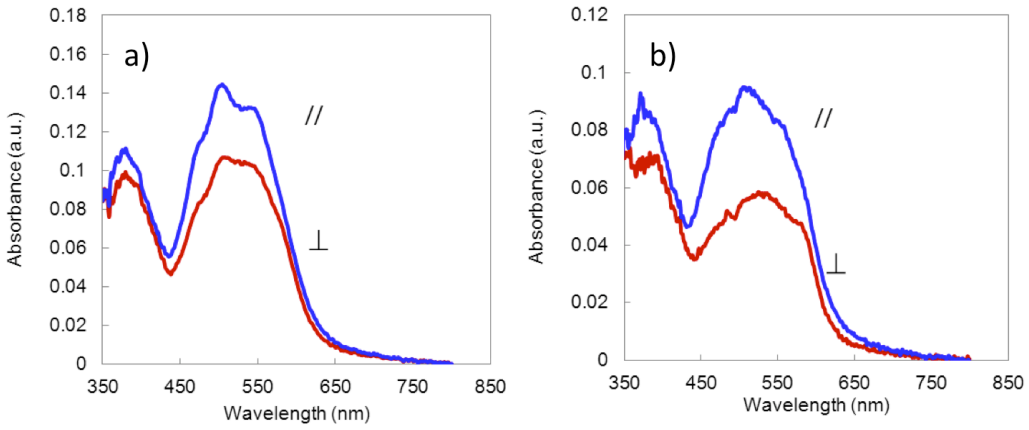

***Figure ESI 2**: Polarized UV-vis spectra of a thin film of AD_0 co-oligomers before (a) and after annealing at 210°C (b). // and ⊥ symbols refer to the orientation of the rubbing parallel and perpendicular to the orientation of the light polarization.*

Figure ESI1 shows the polarized UV-Vis absorption spectra and the polarized optical microscopy (POM) images (c and d) of AD_1 thin film rubbed at T=100°C (Figure ESI 1.a) and after post-rubbing annealing at 190°C (close to the crystallization temperature of AD_1) (Figure ESI 1.b). The UV-Vis spectra of rubbed AD_1 films shows some anisotropy, with a higher absorption when the light polarization is parallel to the rubbing direction **R.** The molecular long axis is aligned more or less parallel to the rubbing direction. The dichroic ratio is in the range of 1.5 to 2 at the maximum of absorption and does not substantially increase after annealing. The UV-Vis spectrum of the rubbed film is dominated by the 500 ($S_{0\text{-}1}$) and 536 nm ($S_{0\text{-}0}$) peaks of the non-aggregated PDI block and the 428 nm peak of the donor block. Although the birefringence suggests some alignment of the co-oligomer, electron diffraction does not reveal any sign of organization (see Figure ESI 3.a). Clearly, no long range order of the co-oligomers is observed in rubbed films. Interestingly, after annealing at 190°C, the rubbed films still show a strong birefringence indicative of in-plane orientation but the UV-Vis absorption spectrum is modified. The change of the vibronic structure associated to the PDI block is indicative of aggregation and strong π-stacking (a similar behavior has been observed for AD_0 and ADA (see Figure ESI2)).[9] The evidence for the aggregation of the PDI block is confirmed by TEM that shows a well-defined self-assembled lamellar mesophase with a characteristic ED pattern.

Figure ESI 3.b shows a representative ED pattern of the highly oriented AD_1 thin film after rubbing and annealing. The sequence of equatorial reflections is associated with the lamellar mesophase and indexed as (0 0 *l*) reflections (*l* = 1-4) (the **c** axis corresponds to the layer normal). It indicates that the lamellar plane is perpendicular to the rubbing direction. In addition, the ED pattern shows two intense and broad reflections at 3.35 Å and located at ±15° from the meridian (this broad reflection corresponds to the overlap of (0 2 *l*) reflections). The π-stacking axis is along the **b** axis of the AD_1 structure. This reticular distance is characteristic of the π-stacking of the co-oligomer molecules as it matches the commonly observed value of π-stacking in PDI-based systems.[10]

The growth of the oriented lamellar structure as a function of temperature was followed in an *in-situ* TEM experiment used for the annealing. Figure ESI 3.c shows the line profiles of the ED pattern along the equator upon heating and cooling of the sample. Lamellar order is manifested by the (0 0 l) (l = 2, 3 and 4) reflections when the temperature approaches the melting temperature (195°C). It becomes more predominant when cooling the samples to room temperature as indicated by the increased peak intensity of the (0 0 l) reflections. The positions of the (0 0 l) reflections do not change on cooling. The lamellar period thus remains essentially constant with temperature. This *in situ* experiment indicates that AD_1 molecules pre-oriented by rubbing, nucleate the growth of oriented lamellae upon annealing close to the crystallization temperature. This implies that the in-plane orientation induced upon high-T rubbing is not lost even when the films are annealed close to the melting temperature.

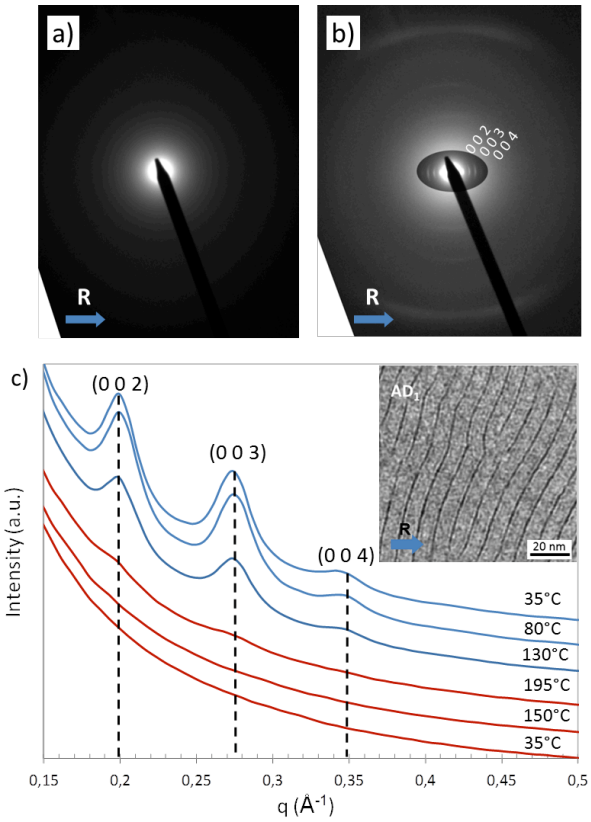

Figure ESI 3: *a and b) ED pattern of a rubbed AD_1 film before and after annealing to 195°C. c) In situ TEM experiment showing the evolution of the intensity of the equatorial reflections in the ED pattern of a rubbed AD_1 film upon annealing to 195°C (red curves) and subsequent cooling (blue curves) to room temperature. The curves correspond to the section profile of the ED pattern along the equator. The successive line profiles were shifted along the ordinate axis to clarify the figure. Inset shows a bright field image of the periodic lamellar structure obtained after annealing of rubbed AD_1 films.*

b) Detailed interpretation of the ED patterns of rubbed co-oligomer films.

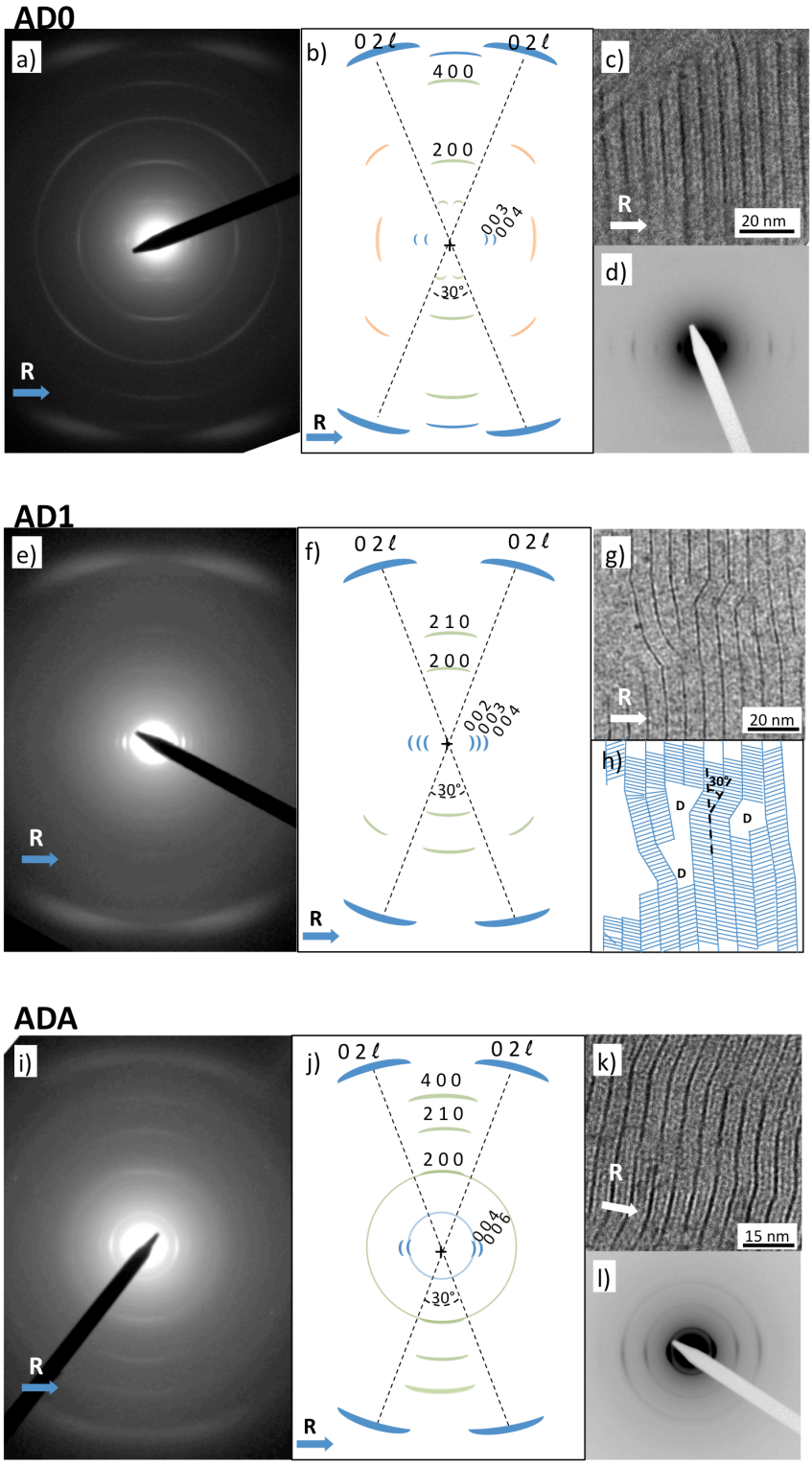

Figure ESI 4: *Typical ED patterns of rubbed a) AD_0, e) AD_1 and i) ADA co-oligomer thin films. b, f, j) Schematic representations of the ED patterns. c, g, h) BF-TEM showing the lamellar structure of AD_0, AD_1 and ADA, respectively. h) Schematic illustration of the orientation of the co-oligomer*

molecules in the lamellae seen in the BF image in g). Characteristic edge-dislocations are highlighted by the letter D. d, l) Low angle diffraction patterns.

Figure ESI 4 shows the ED patterns, the lamellar morphology in bright field (BF) and the low angle electron diffraction (LAED) patterns of AD_0, AD_1 and ADA rubbed and annealed films. Figure ESI 4 shows also schematic illustrations to rationalize the complex ED patterns. The ED pattern shows: i) the sequence of (0 0 *l*) reflections along the rubbing direction, ii) the arced (0 2 *l*) reflections at ±15° from the meridian. The off-meridional position of this reflection indicates that the stacking direction of the molecules is not perpendicular to the lamellae but tilted at ±15° with respect to the normal to the plane of lamellae. A further manifestation of this tilt is illustrated by a close look at typical stacking defects. (Figure ESI 4.g and 4.h). Typical edge dislocations (D) characteristic of lamellar systems are observed that correspond to a twin plane – in effect to a bifurcation of the π-stacking direction while the molecular long axis direction is maintained. The bifurcations make an angle of 2x15° across the twin planes.[11] This ED pattern gives evidence for a first population of crystalline domains such that the long axis and the π-stacking direction of the co-oligomers both lie in the plane of the substrate. For these crystalline domains, the conjugated plane of the co-oligomer is in "edge-on" orientation on the SiO_2 substrate. Crystalline domains for which the long axis of the co-oligomer lies in the plane of the substrate are designated hereafter as "standing lamellae" (a single lamella corresponds to a monolayer of co-oligomer molecules organized in a (**a,b**) plane). As seen in Figure 2, such standing lamellae are made of either "edge-on" or "face-on" co-oligomer molecules on the substrate plane. Even though the ED patterns in Figures 2.a and ESI 4.a show that the population of standing lamellae with edge-on oriented molecules is dominant, there are clear indications for the presence of a population of standing lamellae with face-on molecules. Indeed, beside the broad π-stacking reflection, an additional set of weaker reflections oriented

along the meridian and corresponding to reticular distances of 8.8 Å and 4.4 Å. As seen below, the 8.8 Å and 4.4 Å reflections can be indexed as (2 0 0) and (4 0 0) and correspond to reflections along the alkyl side chains of the co-oligomers (**a** axis of the unit cell). These additional reflections correspond to a second population of standing/inclined lamellae (see schematic in Figure 2.f) for which the π-stacking is almost perpendicular to the substrate plane and the co-oligomer molecules are lying "face-on" on the substrate. For AD_0, a third population of oriented domains is evidenced by the presence of 5.7 and 3.8 Å reflections. This population corresponds to crystalline domains for which the long axis of the co-oligomer molecules is close to the normal to the substrate plane and the **a** axis i.e. the direction of alkyl side chains, is oriented along the rubbing direction. Such domains correspond to so-called "flat-on lamellae" (Figure 2.i).

c) Structural analysis by Grazing Incidence X-ray Diffraction (GIXD).

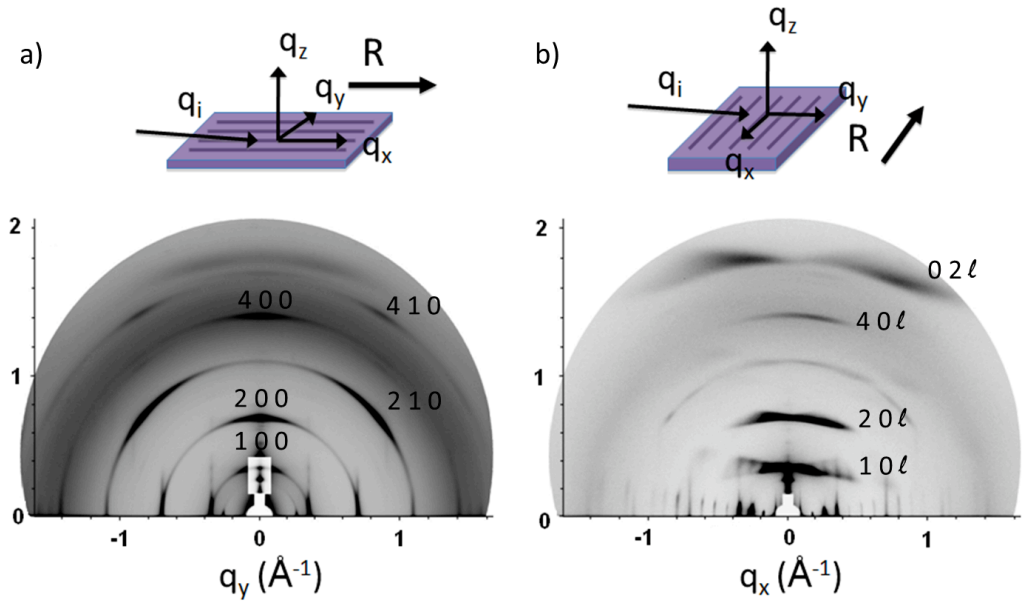

Figure ESI 5: *Two-dimensional grazing incidence X-ray diffraction (GIXD) intensity maps of a rubbed and annealed AD_0 film. a) corresponds to the configuration q_i // R and b) corresponds to $q_i \perp R$ (with q_i, vector of the incident X-ray beam).*

The orientation of the rubbed co-oligomer films was further analyzed by GIXD to obtain additional out-of-plane structural informations. Figure ESI5 depicts the typical 2D maps obtained for two scattering geometries i.e. with the incident X-ray beam oriented either parallel or perpendicular to the rubbing direction. Both patterns reveal the characteristic features of the two populations of standing lamellae with "edge-on" and "face-on" orientations of the co-oligomers as deduced from the ED patterns. For $q_i \perp R$, the sequence of (0 0 *l*) reflections on the equator is clearly seen whereas it is almost absent from the pattern for $q_i // R$ (only the very intense 0 0 3 reflection is observed). Along q_z, one can observe the rather broad (*h* 0 0) reflections with (*h* = 2, 4) that tend to overlap with the close-lying (*h* 0 *l*). Both the equatorial (0 0 *l*) and the (1 0 *l*) reflections are typical fingerprints of the standing lamellae with "edge-on" orientation of the co-oligomers. In contrast, the slightly off-meridional broad reflection at q = 1.9 $Å^{-1}$ corresponds to the set of (0 2 *l*) reflections and is therefore the fingerprint of the standing lamellae with co-oligomers lying "face-on" the substrate. The off-meridional position of these reflections by 15-20° indicates that the π-stacking is not strictly along the normal to the substrate plane but inclined by 15-20°. The GIXD pattern obtained for $q_i // R$ is perfectly consistent with this analysis and contains the contributions of both "edge-on" and "face-on" oriented co-oligomers within standing lamellae.

d) Methodology for structural refinement using a trial-and-error approach.

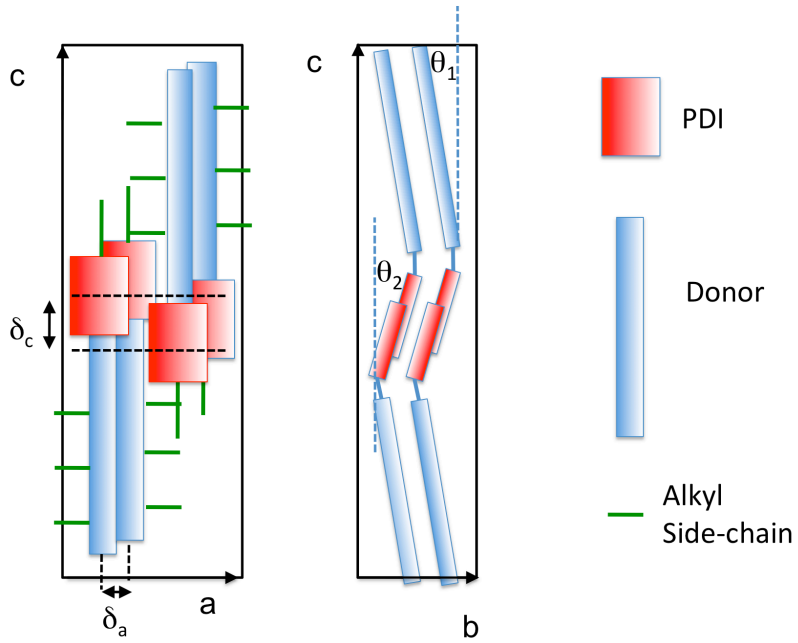

Figure ESI6 : *a) Schematic illustration of the parameters considered for the structural modeling of AD_0 (see text) using the trial-and-error approach.*

Overall, the packing of the co-oligomers in the unit cell must verify a certain number of simple packing/symmetry considerations: i) a strong π-stacking of PDI and donor units in so-called double-layers,[1] ii) an optimized grouping of all alkyl side-chains of the donor block, iii) sufficient space between donor blocks to allow alkyl side-chains to interdigitate.

Having a unit cell and a space group, the structural refinement was performed by a trial-and-error approach similar to that used previously for form I P3HT and PFO.[4,6] The initial molecular conformation of the donor was chosen linear with a planar conjugated backbone[12] (slight twistings between successive blocks forming the donor cannot be excluded). The two thiophene units adjacent to the benzothiadiazole (BT) are placed in *syn* position to each other and they are coplanar with the BT group. The *syn* position of the two thiophenes is imposed by the presence of their ethyl-hexyl side-chains that are both in *anti* position with respect to BT, which should favor molecular packing. The structure of the PDI block is derived from

that found in the literature.[13] Clearly, the exact conformation of the alkyl side-chains is out of reach using this structural refinement procedure and therefore an arbitrary conformation of the branched side-chains is used (which does however allow for the efficient packing of the oligomers in the crystal). For the trial-and-error method, we have used a finite number of geometrical variables defining the conformation of the co-oligomer made of two rigid bodies (the donor and the acceptor blocks), that are: i) the angles θ_1 and θ_2, and the overlap of two co-oligomers in the unit cell along **a** and **c**, and ii) the lateral shifts between successive molecules along **a** and **c**, δ_a and δ_c, respectively (see Figure ESI 4). For the sake of simplicity, rotations of both the donor and the PDI along their molecular long axes (although possible in principle) were not considered hereafter. The possibility of a kink between the A and D blocks was considered in the modeling as well as the tilting of the donor group with respect to the **c** axis of the unit cell by introducing the θ_1 and θ_2 angles. Importantly, the presence of the flexible -$(CH_2)_2$- linker between the D and A blocks allows to tune separately the π stacking distance of the PDIs and of the donor blocks. For the final step of the modeling, X-ray powder diffraction data were also taken into account and the final retained model was the one yielding the best agreement between calculated and experimental patterns for both electron and X-ray diffractions as well as a good agreement between the HR-TEM images and the structural model.

e) Powder diffraction pattern of AD_0.

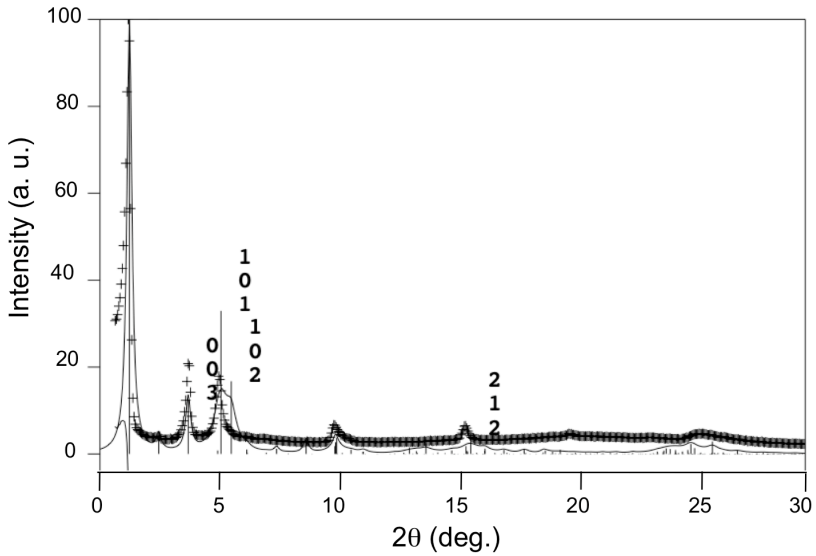

Figure ESI7. Comparison between the experimental (cross symbols) and the calculated powder X-ray diffraction pattern (full line) of the AD_0 dyad structure yielding the best agreement between experimental and calculated ED patterns shown in Figure 4. The dimensions of the crystals for the simulation of the powder diffraction pattern were (l_a=10 nm, l_b=5 nm and l_c=35 nm). No preferential orientation of the powder was taken into account.

f) Observation of the oriented lamellar mesophases by TEM dark field.

The standing lamellae can also be evidenced in the dark field (DF) mode. The DF images shown in Figure ESI 8 are obtained by selecting the very intense (0 2 *l*) reflections observed for all rubbed films (highlighted by a circle in Figure ESI). As expected, the DF images display bright crystalline domains, made of assemblies of 3-5 standing lamellae separated by sharp and dark boundaries. Along the π-stacking direction, the dimension of the lamellae is typically 100 nm for AD_0. It is worth mentioning that the entire lamellae are seen in the DF image, demonstrating that the 3.35-3.5 Å broad reflection corresponds to a π-stacking

distance characteristic of both the PDI and the donor blocks in agreement with the subsequent structural model of the AD_0 packing (*vide infra*).

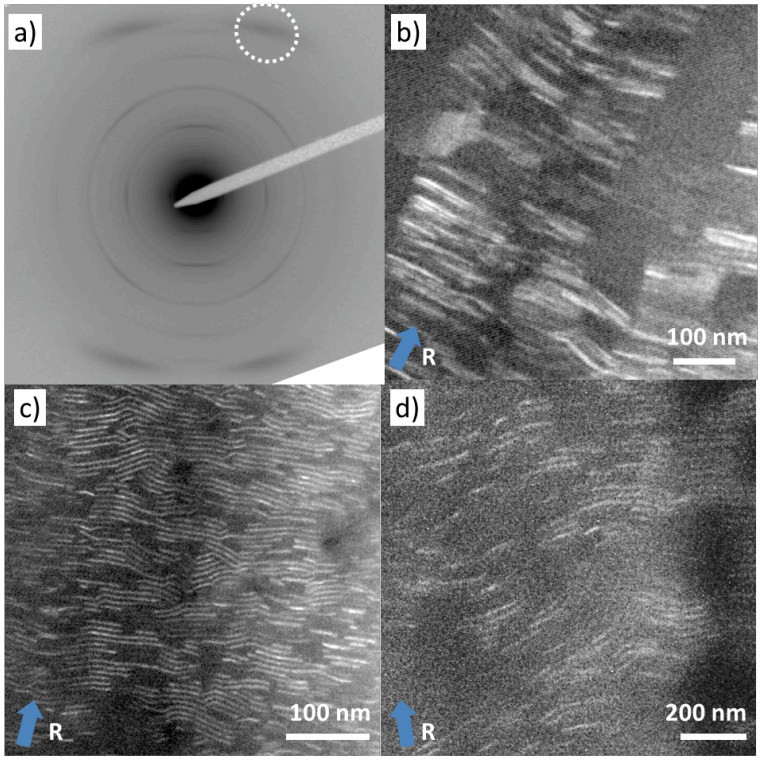

Figure ESI 8: *Dark Fields images of b) AD_0, c) AD_1 and d) ADA thin films obtained by selecting the most intense (0 2 l) series of reflection (white circle) in the ED pattern shown in a).*

g) ED patterns and morphology in AD_1 and ADA films oriented on PTFE substrates.

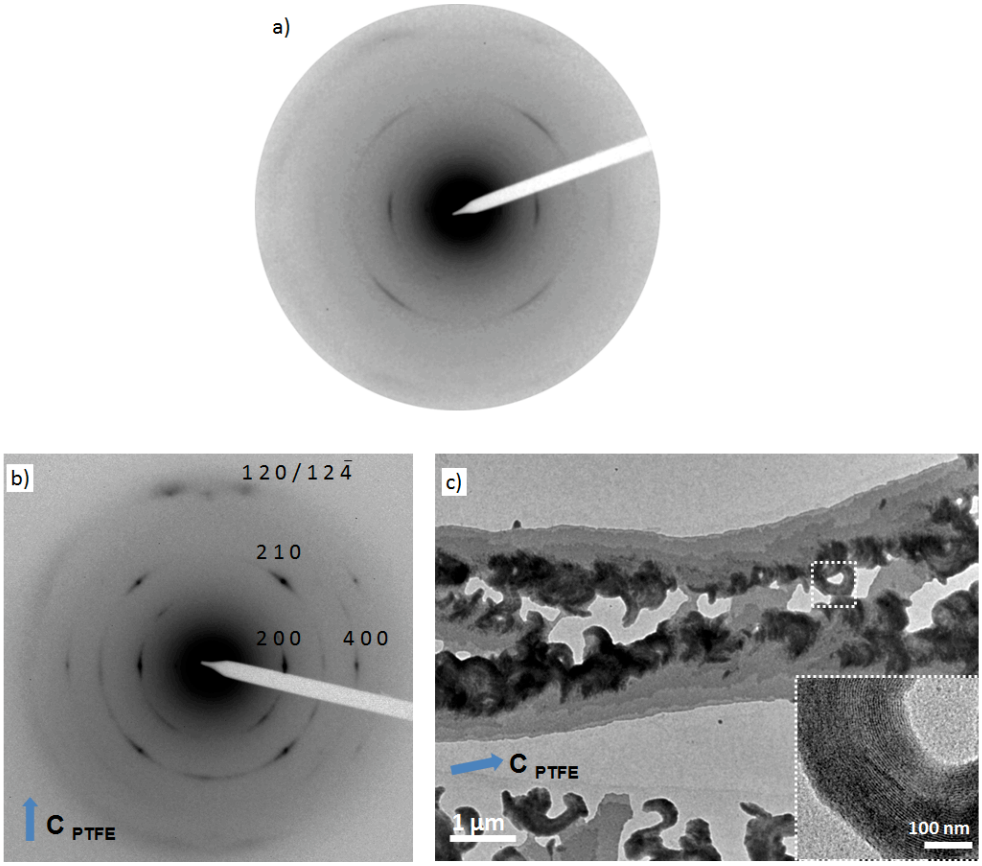

Figure ESI 9: a) Electron diffraction pattern of an oriented AD_1 film on PTFE substrate. b) SAED pattern of ADA film oriented on PTFE substrate, c) BF-TEM images of the flat-lying lamellae on oriented PTFE. The polymer chain axis direction of PTFE is indicated by a blue arrow. Inset in b) show standing lamellae.

Table ESI 1 : *Measured reticular distances from ED and powder XRD patterns with Miller indices h k l of the most intense reflections.*

	AD_0		**AD_1**		**ADA**		**hkl**
Intensity*	d_{hkl} (Å) ED	d_{hkl} (Å) XRD	d_{hkl} (Å) ED	d_{hkl} (Å) XRD	d_{hkl} (Å) ED	d_{hkl} (Å) XRD	
VS	69	70.8	86	96.3			0 0 1
W	34.5	35.3	43	48.5	58	58.8	0 0 2
S	23	23.4	29	32.1			0 0 3
			21	24.0	29	29.3	0 0 4
							0 0 5
				19.4	19	19.7	0 0 6
S	17.4	17.4		17.3		18	1 0 1
M	9.0	8.85	8.7	8.81	8.7	8.79	2 0 0
M	5.75	5.7	5.5	5.7	5.5	5.7	2 1 0
VS		4.5		4.5	4.3	4.5	$h_{ch}+h_{Fluo,PT}+h_{Pery}$
W	4.5	4.44	4.35	4.44			4 0 0
		3.8		3.8			4 1 0
	3.6	3.5	3.4	3.5		3.5	0 2 0
	3.4	3.32		3.32	3.35	3.34	0 2 *l*

* Definition of abbreviations in column 1: VS: very strong, S: strong, M: medium, W: weak.

References.

1) Schwartz, P.-O. ; Zaborova, E. ; Biniek, L. ; Heinrich, B. ; Brinkmann, M. ; Leclerc, N. and Mery, S. *J. Am. Chem. Soc*. **2014**, *136*, 5981−5992.

2) (a) Brinkmann, M.; Pratontep, S. ; Chaumont, C. and Wittmann, J.-C. *Macromolecules*, **2007**, 40, 7532. (b) Vergnat, C.; Legrand, J.-F.; Brinkmann, M. *Macromolecules*, **2011**, 44, 3817. (c) Vergnat, C.; Landais, V.; Combet, J.; Vorobiev, A.; Konovalov, O.; Legrand, J.-F.; Brinkmann, M. *Organ. Elect.* **2012**; (d) Biniek, L.; Leclerc, N.; Heiser, T.; Bechara, R. and Brinkmann, M. *Macromolecules* **2013**, 46, 4014−402.

3) Brinkmann, M.; Graff, S.; Straupé, C.; Wittmann, J.-C.; Chaumont, C.; Nuesch, F.; Aziz, A.; Schaer, M. and Zuppiroli, L. *J. Phys. Chem. B* **2003,** *107* (38), 10531-10539.
4) Kayunkid, N.; Uttiya, S.; Brinkmann, M. *Macromolecules* **2010**, 43, 4961-4967.
5) Brinkmann, M.; Rannou, P. *Macromolecule*s, **2009**, 42, 1125.
6) Brinkmann, M. *Macromolecules* **2007**, 40, 7532.
7) (a) Bunk, O.; Nielsen, M. N. ; Sœlling, T. I.; Van De Craats, A. M.; Stuzmann, N. *J. Am. Chem. Soc.* **2003**, *125*, 2252-2258. (b) Gill, R. E.; Hadziioannou, G.; Lang, P.; Garnier, F.; Wittmann, J.-C. *Adv. Mat.* **1997**, *4*, 331-339. (c) Culligan, S. W.; Geng, Y.; Chen, S. H.; Klubek, K.; Vaeth K. M.; Tang, C. W. *Adv. Mat.* **2003**, *15*, 1176-1180.
8) (a) Biniek, L.; Leclerc, N.; Heiser, T.; Bechara, R.; Brinkmann, M. *Macromolecules* **2013**, *46*, 4014-4023 ; (b) Hartmann, L.; Biniek, L.; Tremel, K.; Kayunkid, N.; Brinkmann, M. *Macromol. Rapid. Commun.* **2014**, *35*, 9-26. (c) Hartmann, L.; Tremel, K.; Uttiya, S.; Crossland, E.; Ludwigs, S.; Kayunkid, N.; Vergnat, C.; Brinkmann, M. *Adv. Funct. Mater.* **2011**, *21*, 4047–4057. (d) Biniek, L.; Poujet, S.; Djurado, D.; Gonthier, E.; Tremel, K.; Kayunkid, N.; Zaborova, E.; Crespo-Monteiro, N.; Boyron, O.; Leclerc, N.; Ludwigs, S.; Brinkmann, M. *Macromolecules* **2014**, *47*, 3871-3879.
9) (a) Gao, F.; Zhao, Y. and Liang, W. Z. *J. Phys. Chem. B* **2011**, *115*, 2699-2708 ; (b) Seibt, J.; Marquetand, P.; Engel, V.; Chen, Z.; Dehm, V. and Würthner, F. *Chem. Phys.* **2006**, *328*, 354-362.
10) (a) Struijk, C. W.; Sieval, A. B.; Dakhorst, J. E. J.; van Dijk, M.; Kimkes, P.; Koehorst, R. B. M.; Donker, H.; Schaafsma, T. J.; Picken, S. J.; van de Craats, A. M.; Warman, J. M.; Zuilhof, H.; Sudho1lter, E J. R. *J. Am. Chem. Soc.* **2000**, *122*, 11057-11066 ; (b) Nolde, F.; Pisula, W.; Müller, S.; Kohl, C.; Müllen K. *Chem. Mater.* **2006**, *18*, 3715-3725.
11) Vergnat, C.; Legrand, J.-F.; Brinkmann, M. *Macromolecules*, **2011**, *44*, 3817-3827.
12) (a) Pasini, M.; Destri, S.; Botta, C.and Porzio, W. *Mat. Sci. and Engin. C* **2002**, *19*, 37-39 ; (b) Pati, P. B.; Senanayak, S. P.; Narayan, K. S. and Zade, S. S. *ACS Appl. Mater. Interfaces* **2013**, *5*, 12460-12468 ; c) Biniek, L.; Fall, S.; Chochos, C. L.; Anokhin, D. V.; Ivanov, D. A.; Leclerc, N.; Lévêque, P.; Heiser, T. *Macromolecules* **2010**, *43*, 9779-9786.

13) (a) Briseno , A. L.; Mannsfeld , S. C. B.; Reese, C.; Hancock, J. M.; Xiong, Y.; Jenekhe, S. A.; Bao, Z. and Xia, Y. *Nano Lett.* **2007**, *7*, 2847-2853 ; (b) Mizuguchi, J. *Acta Cryst.* **1998**, *C54*, 1479-1481 ; (c) Mizuguchi, J.; Hino, K.; Tojo, K. *Dyes and Pigments* **2006**, *70*, 126-135. (d) Percec, V.; Peterca, M.; Tadjiev, T.; Zeng, X.; Ungar, G.; Leowanawat, P.; Aqad, E.; Imam, M. R.; Rosen, B. M.; Akbey, U.; Graf, R.; Sekharan, S.; Sebastiani, D.; Spiess, H. W.; Heiney, P. A.; Hudson, S. D. *J. Am. Chem. Soc.* **2011**, *133*, 12197-12219 ; (e) Dössel, L. F.; Kamm, V.; Howard, I. A.; Laquai, F.; Pisula, W.; Feng, X.; Li, C.; Takase, M.; Kudernac, T.; De Feyter, S.; Müllen, K. *J. Am. Chem. Soc.* **2012**, *134*, 5876-5886 ; (f) Percec, V.; Sun, H.-J.; Leowanawat, P.; Peterca, M.; Graf, R.; Spiess, H. W.; Zeng, X.; Ungar, G.; Heiney, P. A. *J. Am. Chem. Soc*. **2013**, *135*, 4129-4148.